WATER RESOURCES RESEARCH, VOL. 34, NO. 7, PAGES 1795–1807, JULY 1998

Study of spatial scaling in braided river patterns using synthetic aperture radar imagery

Deborah K. Nykanen, Efi Foufoula-Georgiou, and Victor B. Sapozhnikov

St. Anthony Falls Laboratory, University of Minnesota, Minneapolis

Abstract. Synthetic aperture radar (SAR) imagery offers an appealing way of remotely monitoring the complex and rapidly changing forms of braided rivers. These rivers are often found in scarcely inhabited regions and are so dynamic that in situ measurements are almost impossible. In this paper, SAR imagery was used to extract braided river patterns such that their spatial scaling characteristics could be studied. From analysis of several reaches of a braided river in Alaska (the Tanana River), self-affine spatial scaling of the river patterns was found to be present under different flow rates and in different seasons when the river was undisturbed (free of external topographic controls). In regions where predominant geologic controls (i.e., mountains) or predominant flow paths (several tens of times the size of the other channels) were present, no spatial scaling was found. When scaling was found, the values of the anisotropic scaling exponents ν_x and ν_y had very similar values to those found by *Sapozhnikov and Foufoula-Georgiou* [1996] from traced and digitized aerial photographs of several braided rivers.

1. Introduction

Braided rivers consist of numerous alluvial channels that divide and rejoin around bars and islands, forming an intertwining structure that resembles a braid. The dynamic nature of a braided river causes these channels to shift and migrate across the river's braidplain. It is this dynamic nature that makes braided rivers both interesting and difficult to study, especially in a quantitative way. However, the need to build bridges across sections of braided rivers, to harvest the rich mineral deposits left on their bars and banks, and to study the ecological effects of the migrating channels has developed a pressing need for quantitative understanding and prediction of these complex hydrogeomorphological systems and their evolution.

There are several ways in which such large, complex systems could be quantitatively approached. Most research on braided rivers to date has concentrated on understanding the small-scale processes such as flow and sediment flux around an individual channel bar or confluence [*Ashmore and Parker*, 1983; *Ashmore et al*., 1992; *Best*, 1986, 1988; *Bristow et al*., 1993; *Mosley*, 1976, 1977; *Robert*, 1993]. These detailed studies of processes in a small area are valuable but do not necessarily lead to improved understanding of the mechanics of the entire system. Physically based studies and mechanistic modeling of braided rivers aimed at understanding the entire system would be too computationally intensive. A full solution of the governing equations for flow around a single confluence is intensive, and a braided river reach involves many such converging and diverging flow regimes around its numerous bars and islands. Also, there is relatively little quantitative information on how changes in one part of the system propagate to other parts and on which components of the small-scale flow and sediment dynamics contribute to the overall behavior of the system.

Recently, some alternative approaches to studying the morphology and dynamics of braided rivers have been proposed. These type of studies aim to determine which physical processes are critical and how they affect the dynamics of the system as a whole and then concentrate on detailed studies of these processes. *Murray and Paola* [1994] developed a cellular automaton model of a braided river using a simple, deterministic approach of water flow over a cohesionless bed. Their model reproduced the main spatial and temporal features of natural braided rivers. Their results suggested that the main factors essential for braiding were bedload sediment transport and laterally unconstrained free-surface flow. *Sapozhnikov and Foufoula-Georgiou* [1996, 1997] have shown that an effective and fruitful way to study interactions of small-scale and large-scale dynamics of complex natural systems is via statistical scaling analyses, i.e., analyses aimed at determining how morphological or dynamical properties of the system at one scale relate to those at another scale. Such scaling relationships are commonly found in natural systems, including single channels and river networks [e.g., *Tarboton et al*., 1988; *La Barbera and Rosso*, 1989; *Nikora*, 1991; *Sapozhnikov and Nikora*, 1993; *Peckham*, 1995; *Beauvais and Montgomery*, 1996] but have not yet been fully developed or understood in braided rivers. Braided river systems manifest themselves over a large range of scales (e.g., from the smallest channels of a few meters to the whole braidplain width of tens of kilometers). The issue of scale is an essential element when applying the knowledge gained from a small part of a braided river to a larger part of it, from one braided river to another of different size, or from a laboratory model to a real braided river.

Sapozhnikov and Foufoula-Georgiou [1996] found, through analysis of the spatial structure of traced, digitized aerial photographs, that spatial scaling exists in the morphology of natural braided rivers. Spatial scaling implies that morphological properties (e.g., area covered by water) of the system at one scale relate to those at another scale via a transformation which involves only the ratio of the two scales. Through the production of a laboratory braided river in a small experimental facility (0.75 m × 5 m) at the St. Anthony Falls Laboratory,

Paper number 98WR00940.
0043-1397/98/98WR-00940$09.00

Sapozhnikov and Foufoula-Georgiou [1997] also found the presence of scaling in the temporal evolution of braided rivers, called dynamic scaling. Dynamic scaling implies that space and time can be appropriately rescaled such that the evolution of the spatial structure of a small part of a braided river is statistically indistinguishable from that of another larger part or of the whole river. Such relationships could be used, for example, to statistically predict large less frequently occurring changes in the river from smaller more frequent changes or could be used to make inferences about the underlying physical mechanisms controlling the evolution of braided rivers [e.g., see *Sapozhnikov and Foufoula-Georgiou*, 1997, section 5].

It is imperative that the above findings of dynamic scaling are further investigated and that the presence of spatial scaling is further verified using a wide range of natural braided rivers. Braided rivers often exist in scarcely inhabited, high-latitude, glaciated areas and are also constantly evolving, which makes it difficult to perform any sort of ground-based measurements. Also, obtaining aerial photographs at an adequate temporal resolution is difficult and often prohibiting for a single investigator. On the other hand, remote sensing is an attractive means of continually monitoring these complex systems from space. The technology of synthetic aperture radar (SAR) imagery has opened a door of opportunity in the area of quantitative studies of braided rivers, but only a very few studies have existed to date [e.g., *Smith et al*., 1995, 1996]. The scope of this research is to investigate further the presence of spatial scaling relationships in natural braided river patterns using SAR imagery and to explore how this scaling might be affected by flow rate, braiding index, and large-scale topographic controls, such as mountains.

2. Extraction of Braided River Patterns From SAR Imagery for Quantitative Scaling Analysis

The SAR, being carried on an aircraft or spacecraft platform (i.e., satellite), transmits a signal toward Earth at an incidence angle and then measures how much of the signal is echoed back (called backscatter). The backscatter depends on the dielectric properties and surface roughness of the material on Earth being scanned by the radar. SAR's independence of solar illumination and cloud cover makes it especially useful in providing consistent seasonal and diurnal coverage, which is hard to do with aerial photographs or other remote sensors. Each pixel in a SAR image represents the radar backscatter for the area on the ground covered by that pixel. The radar backscatter is recorded as a brightness value, or intensity, which in a gray-scale mode ranges from 0 to 255. Brightness values in the lower end of the range (i.e., dark) are recorded for low radar backscatter, and values in the upper end of the range (i.e., bright) are recorded for high backscatter. In general, rough ground surfaces cause bright pixels, and smooth ground surfaces cause dark pixels in the image. Brightness increases with the wetness of the object, except for the case of a smooth (i.e., calm) body of water, which will appear dark. (See http://www.asf.alaska.edu, *Oliver* [1991], and *Olmsted* [1993] for more information on SAR imagery and its interpretation.)

In this study, SAR imagery acquired by the first European Remote Sensing Satellite (ERS-1) was used. ERS-1 was launched on July 17, 1991, by the European Space Agency (ESA). It carries a C-band (5.66 cm wavelength) SAR and has a spatial resolution of 30 m with a pixel spacing of 12.5 m and coverage of a 100 km $\times$ 100 km area in each image. The images used for this study were ERS-1 full-resolution images collected over the Tanana River in May through October of 1993. They were provided by the ESA and acquired through the Alaska SAR Facility (ASF).

The methodology for extracting the braided river patterns from the SAR images is based on the property of smooth bodies of water appearing dark. Although this may work well for single-channel rivers, the conditions of wet gravel on bars and banks and changes in backscattering intensity for narrower, shallower channels make it difficult to delineate active channels in braided rivers [*Smith et al*., 1996]. The method of extraction developed here deals with these difficulties by combining a series of automated and manual steps and is therefore referred to as a semiautomated procedure. The method is broken down into four stages: (1) image processing, (2) image enhancement, (3) image classification, and (4) postimage processing.

2.1. Image Processing

The first step in working with SAR data is radiometric calibration. This is an adjustment to the brightness values in the image to compensate for the antenna pattern's, range-to-target's, and incidence angle's effect on the signal level. It permits comparison of brightness values between different images and also within a single image. The correction is based on the measured response to aluminum trihedral corner reflectors of known size, shape, orientation, and cross section placed on the ground at strategic locations within the ASF station mask. The ERS-1 SAR images used for this study were radiometrically calibrated using a software program provided by ASF called "calibrate." (See http://www.asf.alaska.edu and *Olmsted* [1993] for more information on radiometric calibration.) Another program provided by ASF called "sarautoreg" was used to automatically geocode the images. Geocoding simply means rotating the image from a swath reference frame, which is orientated along the flight path of the satellite, to a geographic coordinate system.

After the images have been radiometrically calibrated and geocoded they were filtered to reduce speckle noise. Speckle noise is an inherent feature of SAR and is produced when surface variations near the size of the radar's wavelength (e.g., small rocks, leaves, and ripples on a water surface) cause multiple scatters of the radar echo, which when added incoherently give a higher backscattering intensity. This net backscatter makes the object on the surface appear as a bright pixel in the SAR image. Although it is not feasible to completely remove speckle noise, it can be sufficiently reduced and smoothed using filtering algorithms. Through literature review [*Frost et al*., 1982; *Lopes et al*., 1990; *Hagg and Sties*, 1994; *Shi and Fung*, 1994] and informal comparative testing on an image clip, it was determined that the Frost filter [*Frost et al*., 1982], with a 3 $\times$ 3 kernel and a coefficient of variation equal to that computed for the unfiltered image, worked best for suppressing speckle noise while preserving edge structures and linear features. Other filters considered in the informal comparative testing were Lee, Lee-Sigma, Maximum a Posteriori (MAP), and Median. (See *Lopes et al*. [1990] and *Shi and Fung* [1994] for a description of these filters.) Various kernel sizes, coefficients of variation, and numbers of passes were also tested for each filter. The filters were applied using the software package Imagine 8.2, developed and distributed by ERDAS®, Inc.

Following the Frost filter, the images were refiltered using a

2×2 mean filter to further smooth and suppress speckle noise. The images were also rotated so that the upstream and downstream end points of the river reach were vertically aligned, with the upstream end at the top of the image.

2.2. Image Enhancement

Since regions of calm water and other smooth surfaces appear dark in SAR images, ideally, all river channels would appear dark with an associated gray-scale brightness value of 0. However, nonuniform conditions and inconsistencies in backscatter returns cause the brightness values to range anywhere from 0 to 150 (on a scale of 0–255) and even greater in some cases. In order to decipher which pixels are occupied by water and which are not, image enhancement is needed to be able to follow tonal variations in a similar fashion as the human eye does.

The first step in the image enhancement stage was to adjust the contrast levels in the images. This is known as contrast enhancement, and it increases the differences (or contrast) between the reflectivity of two different materials. It is applied by setting all values below a lower threshold to 0 and values above an upper threshold to 255. The values between the upper and lower threshold are then stretched over the 1–254 range. (See *Jensen* [1996] for more information on contrast enhancement.) The most suitable upper and lower thresholds were determined by trial and error for each image, with the upper thresholds typically ranging around 200 and the lower thresholds ranging around 100. (See Appendix A for justification of the subjectivity in the threshold selection.) This linear contrast adjustment worked well for darkening water pixels and brightening nonwater pixels, resulting in an improved braided channel network. Pixels that were part of an active channel and had values below the lower threshold now became uniformly dark with an associated brightness value of 0. The pixels that were also part of an active channel but had values that fell above the lower threshold now had brightness values closer to 0. The SAR images were contrast-enhanced using Adobe Photoshop 3.0.

The next step in the image enhancement stage was to improve the channel connectivity. The technique used was to look at directional averages and fill-in channels (i.e., set their pixel value equal to 0) based on these averages. An algorithm was developed that computed the average brightness value over a user-specified number of pixels away from a center pixel in eight different directions. The direction of the smallest of the eight directional averages was taken as the preferred channel direction. If this smallest average was below a specified minimum average criterion, then the center pixel and a user-specified number of pixels away from the center pixel in the preferred direction (typically smaller than the number of pixels used for the directional averaging) were set equal to 0. The algorithm then moved to the next pixel and repeated the process. The result was an improved braid channel network but not yet completely connected.

2.3. Image Classification

In order to ensure a completely connected braid channel network some manual image manipulation was required. The image classification stage is the "semi" part of the semiautomated extraction procedure. The SAR images were loaded into the graphics program Neopaint 3.2a, developed and distributed by NeoSoft Corporation. The connected braid channels were filled with a user-specified color by clicking the upstream end of a known channel. All connected pixels with brightness values of 0 were automatically filled with the color. The disconnected sections that visually appeared to be part of active channels were then manually filled with the color by following the tonal variations. The degree of subjectivity here was that the user must determine which gaps are truly part of active channels and which are produced by overfill into inactive channels. However, in most cases the tonal variations made this determination fairly clear to the human eye. The result, after approximately 1 hour of manual image cleanup, was a completely connected braid channel network with inactive channels truncated and rough edges smoothed. The image files were then converted to a binary classification scheme where all pixels filled with the color where set equal to 1 (denoting a wet pixel) and all other pixels were set equal to 0 (denoting a dry pixel).

An Unsupervised Bayesian Classification algorithm was tried as an alternative to fully automate the extraction procedure (applied using Imagine 8.2, developed and distributed by ERDAS®, Inc.). However, the result was still a discontinuous channel network. Its performance was less desirable than the above described image-processing stages in that it tended to misclassify numerous nonwater pixels as water and vice versa.

2.4. Postimage Processing

The final stage of the extraction methodology used in this study was to run the binary classified file (i.e., 1s and 0s) through a modified median filter. This was done to further smooth channel edges and fill extraneous point bars. This filter works by counting the number of filled pixels (i.e., value of 1) in a 3×3 kernel. If the total number was ≥ 5 (majority of the box contains water pixels), then the center pixel was set equal to 1 or "wet." If the sum was ≤ 2 (largely a nonwater box), then the center pixel was set equal to 0 or "dry." At this point the image files were now ready for testing the presence of scaling and estimating the spatial scaling exponents.

3. Testing for Spatial Scaling and Estimation of Scaling Exponents

The presence of spatial scaling in an object means that statistical properties at one scale relate to the statistical properties at another scale via a transformation which involves only the ratio of the two scales. This is also known as scale invariance and means that the object is statistically indistinguishable under proper magnification or contraction. When the properties scale similarly in all directions, it is referred to as isotropic scaling, and the object is a self-similar fractal. However, when the properties scale differently in different directions, it is called anisotropic scaling, and the object is a self-affine fractal. *Sapozhnikov and Foufoula-Georgiou* [1995] developed a methodology to test and quantitatively assess the presence of self-affinity in any complex geometrical pattern, such as a braided river, and to estimate the fractal exponents that define its spatial scaling. This method is called the logarithmic correlation integral (LCI) method and is briefly presented here for sake of completeness.

Let X and Y be the sides of a rectangle and $M(X, Y)$ be the mass (e.g., the number of pixels covered by water) of the part of the object contained within the $X \times Y$ rectangle. Then, spatial scaling implies that

$$M(X,Y) \sim X^{1/\nu_x} \sim Y^{1/\nu_y} \tag{1}$$

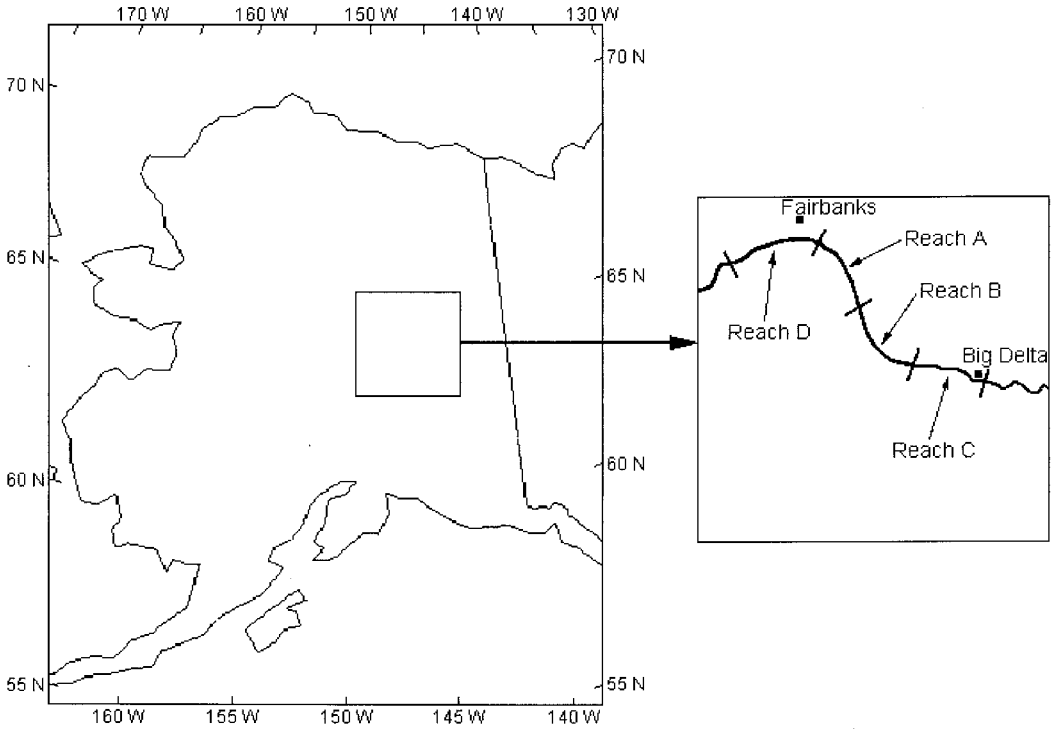

Figure 1. Location of Tanana River, Alaska, and studied sites.

where ν_x and ν_y are the fractal exponents corresponding to the X and Y directions, respectively. This equation can be written in the form

$$\left(\frac{X_2}{X_1}\right)^{1/\nu_x} = \left(\frac{Y_2}{Y_1}\right)^{1/\nu_y} = \left(\frac{M_2}{M_1}\right) \tag{2}$$

If we let $x = \log X$, $y = \log Y$, and $z = \log M$, we get

$$\frac{x_2 - x_1}{\nu_x} = \frac{y_2 - y_1}{\nu_y} = z_2 - z_1 \tag{3}$$

or

$$\frac{dx}{\nu_x} = \frac{dy}{\nu_y} = dz \tag{4}$$

The function $M(X, Y)$ is known as the correlation integral, and by analogy we call the function $z(x, y)$ the logarithmic correlation integral of the object under study. Comparing (4) with

$$\frac{\partial z}{\partial x}\,dx + \frac{\partial z}{\partial y}\,dy = dz \tag{5}$$

we obtain

$$\nu_x \frac{\partial z}{\partial x} + \nu_y \frac{\partial z}{\partial y} = 1 \tag{6}$$

This relationship provides a method for testing the presence of spatial scaling and for estimating the fractal exponents ν_x and ν_y of a self-affine object, as follows. Having estimated the logarithmic correlation integral $z(x, y)$ from a pattern of the object by direct calculation of the mass $M(X, Y)$ (i.e., pixels covered by water) within rectangles of sizes $X \times Y$, one can calculate the derivatives $\partial z(x, y)/\partial x$ and $\partial z(x, y)/\partial y$ and use them to test whether the linear relationship (6) is satisfied and, if yes, to find the values of ν_x and ν_y. As can be seen from the above equation, $1/\nu_y$ is the intercept of the linear best fit line with the vertical axis, and $-\nu_x/\nu_y$ is the slope. Ideally, only two

Table 1. ERS-1 Synthetic Aperture Radar (SAR) Images Used in This Study

ASF Data Identifier	Scene Indicator	Date	Time, UT	River Reaches Contained in Image	Flow Rate, cfs	Braiding Index
E1/S/09807.01	152993100	May 31, 1993	2106:34	A, B, D	35300	4.59, 4.23, 3.23
E1/S/10308.01	208531100	July 5, 1993	2106:39	A	49900	4.75
E1/S/11811.01	152999100	October 18, 1993	2021:47	A, B	unknown	4.06, 3.44
E1/S/10265.01	208527100	July 2, 1993	2101:05	C	51300	5.22
E1/S/10494.01	208588100	July 18, 1993	2058:11	C	60300	5.35
E1/S/10351.01	208533100	July 8, 1993	2112:21	D	49100	3.14

ASF, Alaska SAR Facility.

Table 2. Tanana River Reaches Used in This Study

Reach	Reach Length, km	Upstream Coordinates	Downstream Coordinates
A	28.6	64°34′, −147°04′	64°46′, −147°35′
B	34.25	64°18′, −146°43′	64°34′, −147°04′
C	25.8	64°10′, −145°53′	64°16′, −146°40′
D	32.2	64°35′, −147°40′	64°35′, −148°20′

points are needed to estimate v_x and v_y, but for a good estimation a least squares fit to the derivatives at all points of the surface $z(x, y)$ is preferable. Since both coordinates contain uncertainty in their values it is not appropriate to use the traditional least squares method, which minimizes the sum of the squares of the vertical distances between the fitted line and the actual data points, since this method is sensitive to the orientation of the coordinate system. Thus a method which minimizes the sum of the squares of the perpendicular distances was used. This method was implemented with the revised algorithm of *Alciatore and Miranda* [1995] which is numerically stable and gives a unique solution.

4. Analysis of the Spatial Scaling of the Tanana River, Alaska

The ERS-1 SAR images selected for analysis cover the Tanana River from Big Delta, Alaska, to just past Fairbanks, Alaska, and were taken between May 31 and October 18 of 1993. They were selected to cover various reaches of the Tanana River over different instants of time and flow rates (see Figure 1). Table 1 lists the images analyzed and their corre-

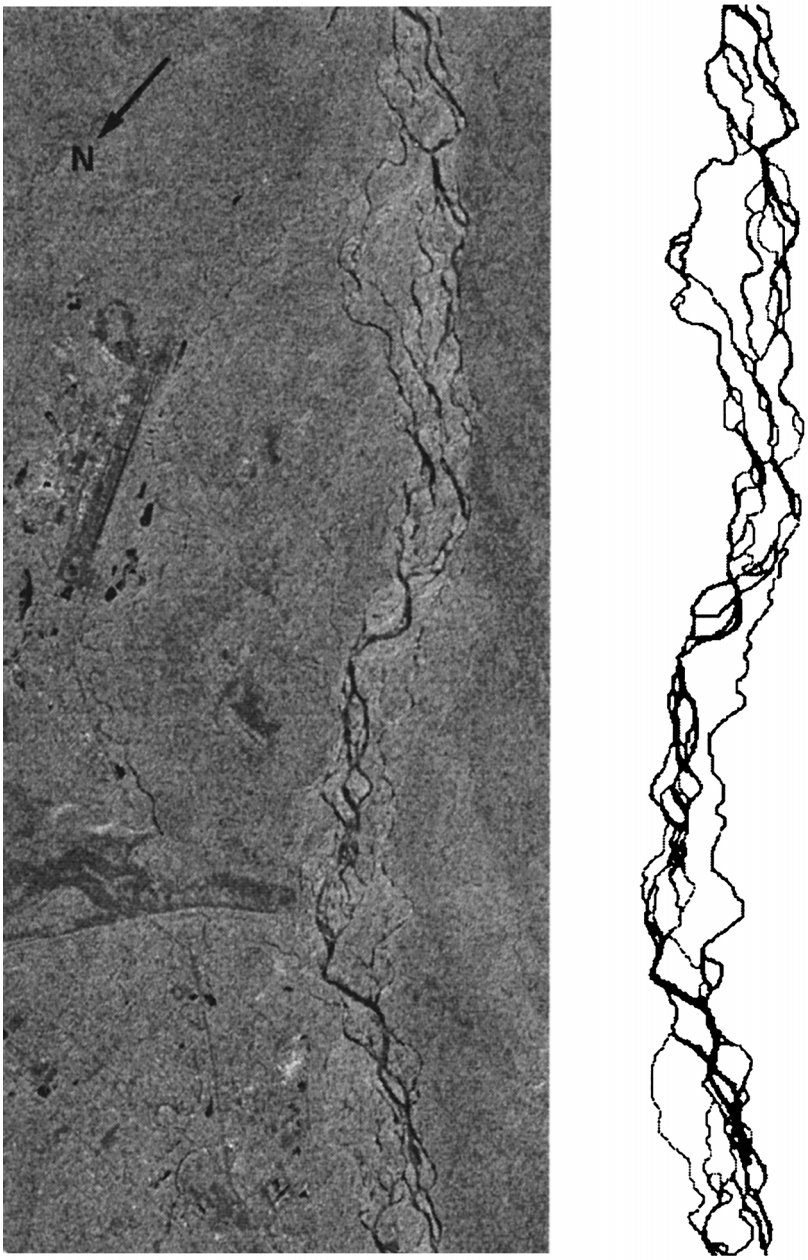

Figure 2. Original synthetic aperture radar (SAR) image and extracted braided river pattern of the Tanana River: reach A, image ID 152999100. Copyright ESA 1993.

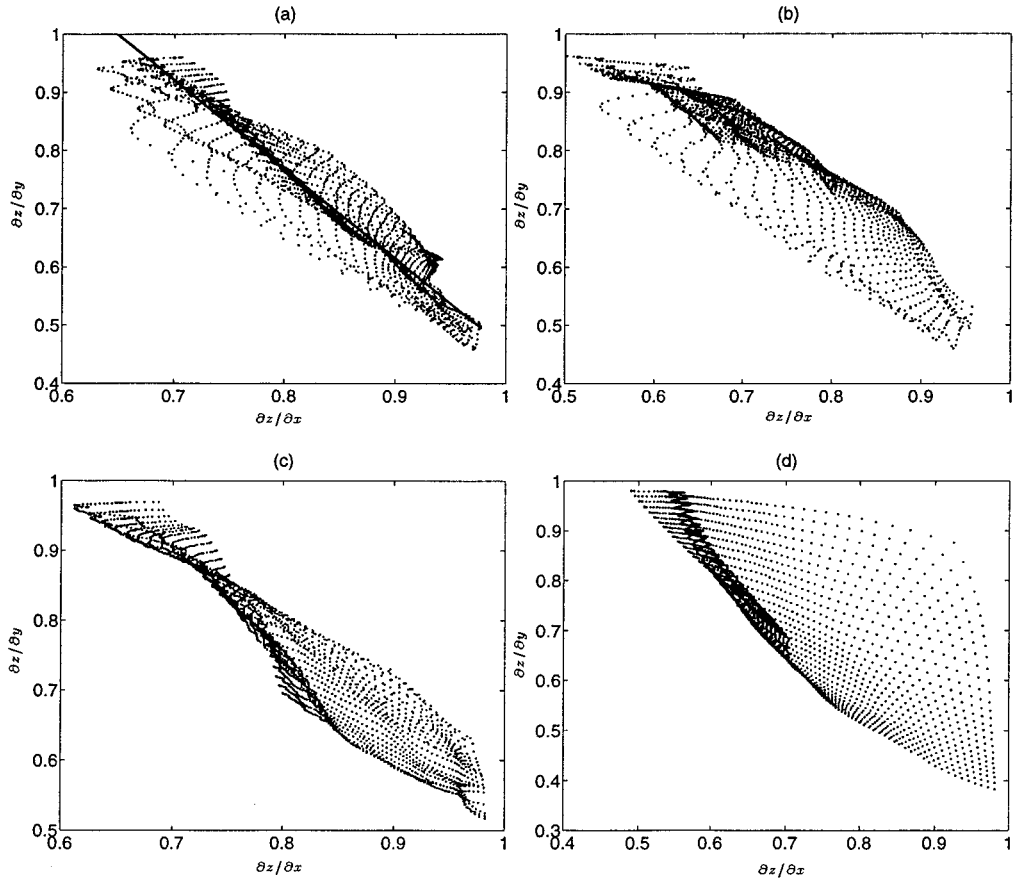

Figure 3. Testing the presence of spatial scaling and estimation of the fractal exponents ν_x and ν_y for the extracted braided river pattern of the Tanana River: (a) reach A, image ID 152999100, (b) reach B, image ID 152993100, (c) reach C, image ID 208527100, and (d) reach D, image ID 208533100.

sponding river reach, date, time, flow rate, and braiding index. Flow rates were obtained from the U.S. Geological Survey (USGS) records and were measured near Fairbanks, Alaska. The braiding index for each river reach was computed as the average number of channels in all cross sections of the extracted pattern. (Note that the braiding index does not reflect the relative width of these channels.) The length and coordinates of the four reaches analyzed are shown in Table 2. The patterns were extracted from each of the SAR scenes using the extraction methodology described in section 2 and validated in Appendix A, and their spatial scaling was analyzed using the logarithmic correlation integral method reviewed in section 3.

Three scenes were analyzed for reach A, the river reach stretching from south of the Eielson Air Force Base to Fairbanks. This reach is 28.6 km in length with an average braidplain width of 1 km and a slope of 0.0011. The original SAR scenes and the extracted braided river patterns for this reach are given by *Nykanen* [1997]. Here only the October 18, 1993, scene of this reach is shown in Figure 2. All three scenes exhibited good scaling within scales corresponding to the width of the smallest individual channels up to the whole braidplain width. We show here the scaling results of only the October 18, 1993, scene (see Figure 3a) and summarize the results for all three scenes in Table 3. The flow rate for the July 5th scene is ~15,000 cfs more than the May 31st scene. The flow rate for the October 18th scene is unknown but was estimated from the method of *Smith et al*. [1996] (see Appendix B) to be 7800 cfs, which is substantially lower than the other two scenes. It is interesting to note that despite the large range in flow rates the spatial scaling stills holds for all three scenes of reach A and with similar scaling exponents. The ν_x and ν_y values were 0.74–0.77 and 0.47–0.50, respectively, as shown in Table 3.

Table 3. Spatial Scaling for the Tanana River, Reach A (South of Eielson Air Force Base to Fairbanks)

Scene Indicator	Date	Flow Rate, cfs	Braiding Index	ν_x	ν_y	Correlation Coefficient	Average |error|	Standard Deviation |error|
152993100	May 31, 1993	35300	4.59	0.74	0.47	−0.929	0.0175	0.0122
208531100	July 5, 1993	49900	4.75	0.70	0.50	−0.844	0.0205	0.0189
152999100	October 18, 1993	7800*	4.06	0.77	0.50	−0.953	0.0158	0.0143

*Flow rate estimated using W_e − Q relationship developed by *Smith et al*. [1996] (see Appendix B).

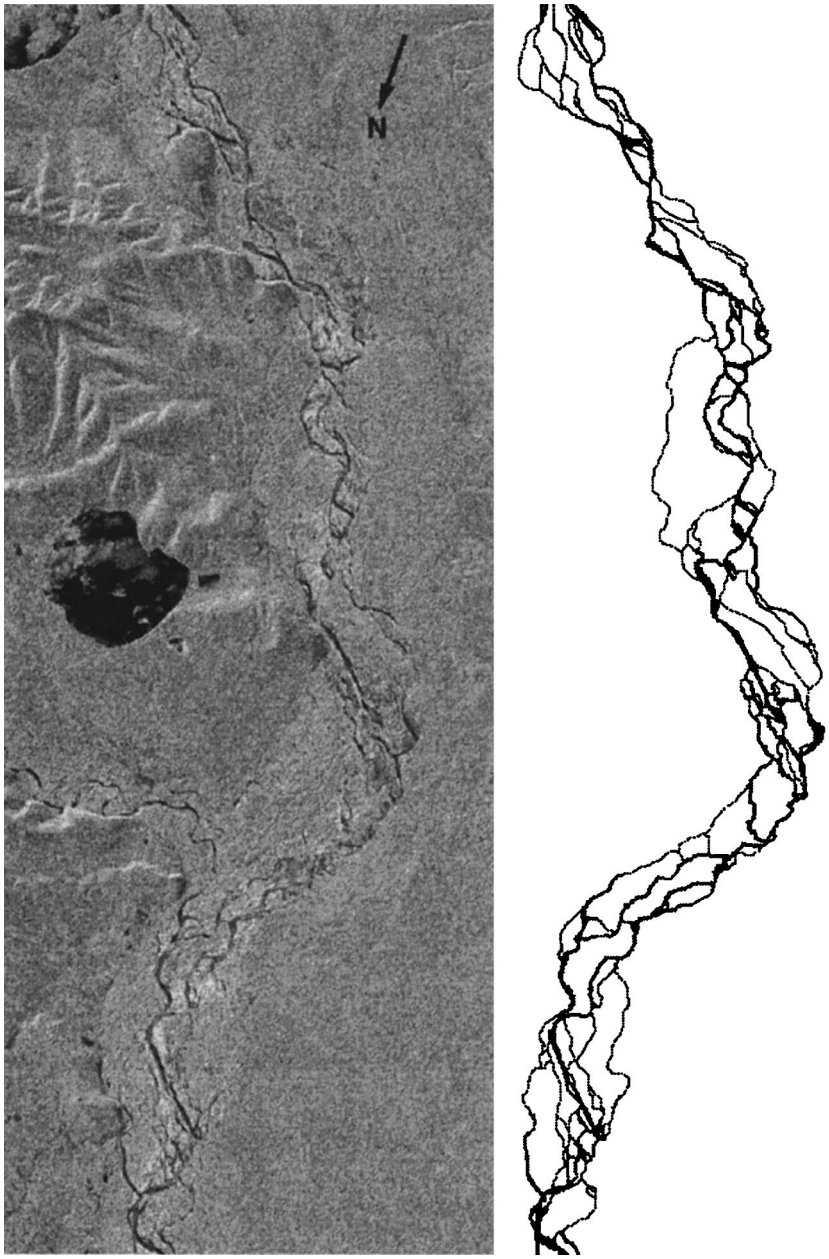

Figure 4. Original SAR image and extracted braided river pattern of the Tanana River: reach B, image ID 152993100. Copyright ESA 1993.

This stability in scaling structure for different flow rates was also found by *Nikora et al*. [1995] in a study of braided rivers as self-similar objects with reported fractal dimension $D = 1.5–1.7$. They found universality of the channel pattern fractal dimension under various water discharge rates for the Ohau River in New Zealand and related this universality to the appearance of new anabranches on big islands compensating the flooding of small islands when the water discharge increases.

Contrary to reach A, reaches B and C of the Tanana River displayed relatively poor scaling for all scenes analyzed. For example, Figures 3b and 3c show the scaling results from the May 31, 1993, scene of reach B and the July 2, 1993, scene of reach C, respectively. Figures 4 and 5 show the SAR images of these reach B and C scenes, respectively. The cloud of points in Figures 3b and 3c are very different from the typical curve of Figure 3a. In both Figures 3b and 3c the main body of the cloud takes on a concave shape. Figures 3b and 3c also lack the fullness and even distribution of points throughout the cloud mass that is seen in Figure 3a. The reason for this poor scaling might be the interaction of the physical mechanisms controlling the braidplain morphology with external factors imposed on the river. In both reaches B and C a mountainous region adjacent to the river affected strongly the path of the river (see Figures 4 and 5 and *Nykanen* [1997] for all scenes of reaches B and C). When the braidplain of a river reach is forced by an external factor, it is definitely other mechanisms besides braiding that control the resulting morphology of the river. It appears that the prerequisite for spatial scaling is that the river is allowed to evolve in a natural, self-organized way such that the spatial structure of the river is determined by the same mechanisms at all scales. Any interference with this self-organization can break the underlying spatial scaling. Indeed, large-

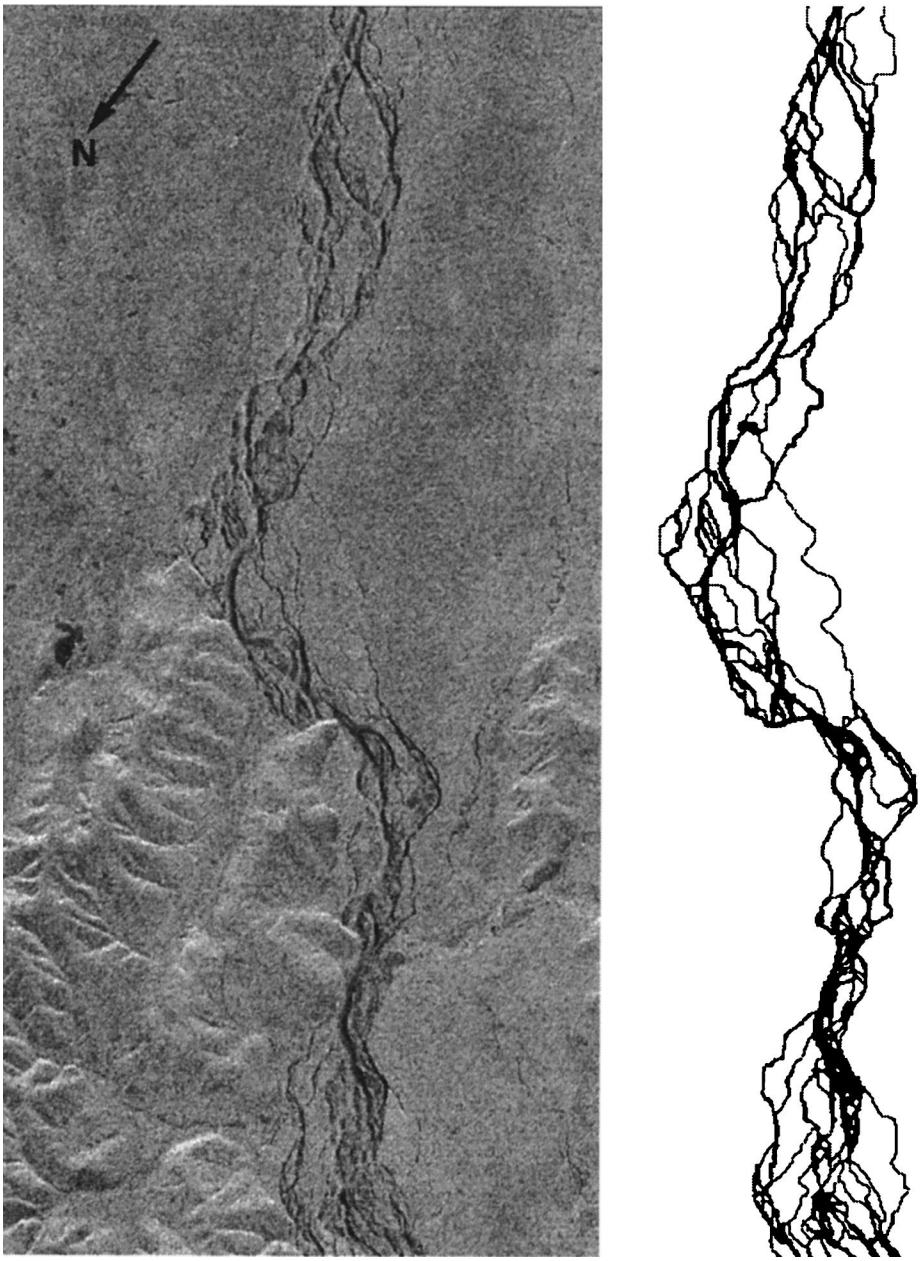

Figure 5. Original SAR image and extracted braided river pattern of the Tanana River: reach C, image ID 208527100. Copyright ESA 1993.

scale perturbations caused by external factors (e.g., mountains) are shown here to affect the scaling properties of the river pattern at all scales (even scales smaller than the scale of the external factor). This holds true, in general, for self-affine objects because they possess anisotropy at all scales but would not be true for self-similar objects. For example, rotating half of a self-similar object by 90° would break the scaling in the object at the scale of the rotation only but not at smaller scales. However, rotating half of a self-affine object by 90° would destroy the scaling anisotropy at all scales.

Reach D, located downstream of Fairbanks, is different from the other reaches in that the slope is more gradual and the braiding index is lower. The original SAR image for the July 8, 1993, scene of this reach is shown in Figure 6. It was found that spatial scaling also did not hold in this reach (see Figure 3d). In this case, however, there appeared to be no morphological constraints that would interfere with self-organization of the braidplain. The reach is characterized by braiding with a predominant channel throughout the reach. The width of this main channel is only 4 times smaller than the whole braidplain width and ~10 times greater than the next biggest channel; that is, channels of intermediate widths are missing from this river reach. Our analysis shows that such rivers, which are braided but have a predominant channel, do not exhibit self-affine scaling. It should be mentioned that lack of scaling here is due to the fact that not enough scales are present to detect scaling. It does not necessarily imply the presence of a different shaping mechanism compared to braided rivers with a large braiding index. Braided rivers with a low braiding index and a predominant flow path (channel width) can be seen as a transitional case between the class of simple meandering rivers and braided rivers with all scales of

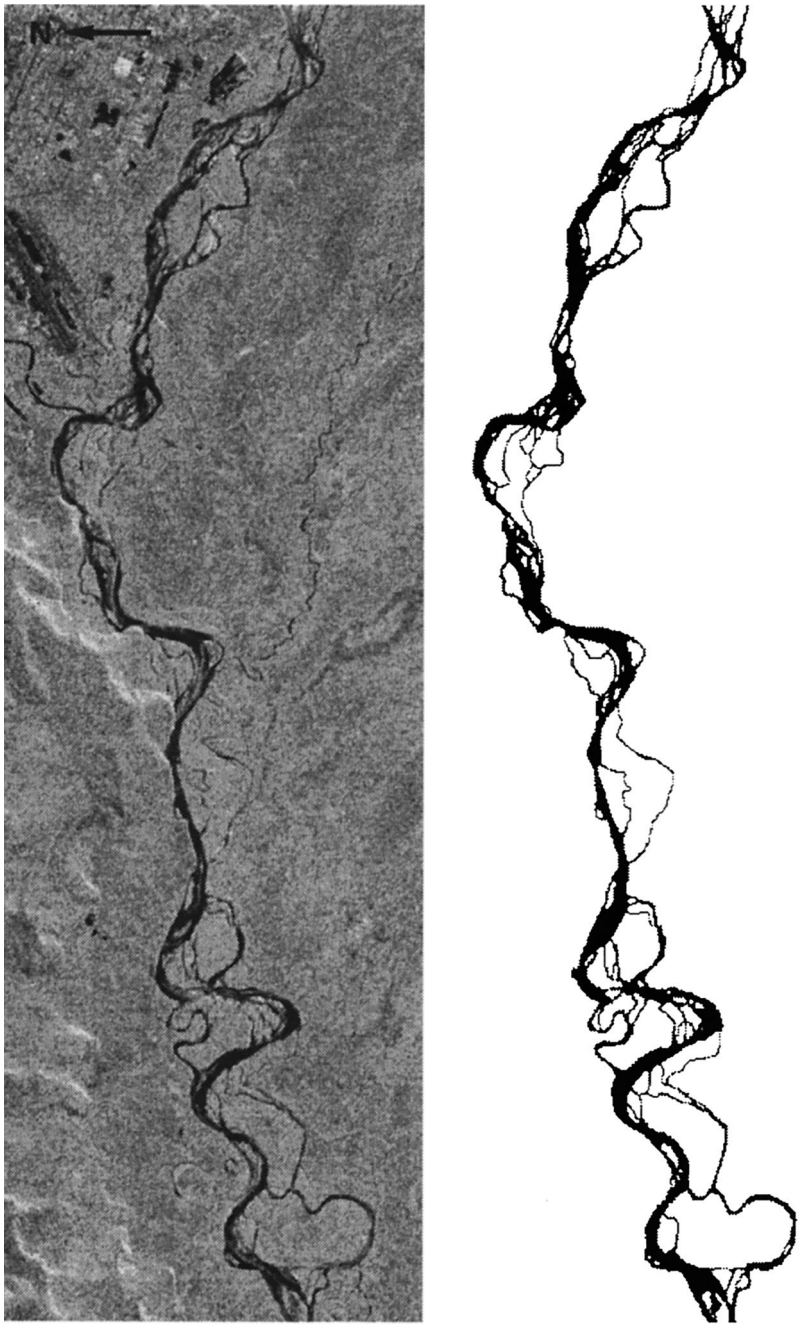

Figure 6. Original SAR image and extracted braided river pattern of the Tanana River: reach D, image ID 208533100. Copyright ESA 1993.

channels present. In fact, reach D is also geographically a transitional river reach, connecting a braided regime (with all scales of channels present) to a single meandering river regime. Note that although self-affine spatial scaling has been found to hold for these two classes of rivers in undisturbed environments (with different scaling exponents) [e.g., see *Sapozhnikov and Foufoula-Georgiou*, 1996, Table 3), it was found here to fail for "transitional rivers," i.e., braided rivers with channels of a few predominant scales only.

5. Conclusions

Several conclusions can be drawn from this study of spatial scaling in braided river patterns from SAR imagery, which are as follows:

1. It was found through this research that a fully automated extraction procedure for extracting braided river patterns from SAR imagery is not feasible because of the limitations of using SAR imagery in a quantitative way. A semiautomated scheme involving several stages of speckle noise reduction, channel enhancement, and some manual image interpretation worked satisfactorily in extracting a reasonable and spatially consistent braid channel network suitable for spatial scaling analysis.

2. Self-affine spatial scaling for braided rivers was found to hold over different flow rates and instants of time when the river was free of topographic controls (e.g., mountains). It was found to be relatively poor in regions where a characteristic of the morphology, mountains in our case, prevents the river from

evolving and developing its braidplain in a natural (undisturbed) fashion.

3. Self-affine spatial scaling behavior was also not found to be present for a braided pattern with a predominant flow path, or main channel, several tens of times the size of the other channels in the braidplain. Lack of scaling in these patterns was argued not to imply necessarily the presence of different shaping mechanisms of braiding compared to braided patterns with enough scales of channel present.

4. Within the scales of its braidplain width and without the presence of morphological constraints the Tanana River was found to exhibit self-affine scaling with fractal exponents $\nu_x = 0.74–0.77$ and $\nu_y = 0.47–0.50$. Previously, *Sapozhnikov and Foufoula-Georgiou* [1996] found spatial scaling exponents of 0.72–0.74 for ν_x and 0.51–0.52 for ν_y from traced and digitized aerial photographs of three natural braided rivers (Brahmaputra River in Bangladesh and Hulahula and Aichilik Rivers in Alaska). The similarity in the exponents found previously to those found in this study is one step further in indicating that the spatial structure of braided rivers may be determined by universal features in the physical mechanisms shaping these rivers.

Although the physical implications and practical utility of scaling relationships are not fully understood yet, unraveling scale invariant relationships from complex natural patterns is interesting in its own right. The fact that these scale invariances in braided rivers seem to be present (and with universal parameters) in undisturbed systems which had the chance to self-organize themselves laterally and vertically to an equilibrium state but are not present in systems subject to other external controls implies that the physical mechanisms responsible for braiding are universal (independent of many specifics of the system like bed material, slope, etc.) and the same over a range of scales. It cannot be determined directly from ν_x and ν_y exactly what these mechanisms are. However, if we believe that self-affinity is a universal property of braided rivers, any physical model of braided rivers should exhibit this property. Thus modeling of braided rivers in conjunction with the revealed self-affinity can provide a powerful tool for understanding the mechanisms responsible for the formation of braided patterns.

More challenging than studying the planform morphology of braided rivers is studying the dynamics of their evolution in terms of space-time scale invariances. Such a study was recently performed by *Sapozhnikov and Foufoula-Georgiou* [1997], who found the presence of dynamic scaling in an experimentally produced braided river. It remains to be seen whether SAR imagery can provide the necessary data needed to verify or dispute the presence of dynamic scaling in natural braided rivers too and subsequently to study the conditions under which such spatiotemporal invariances in braided rivers seem to be present.

Appendix A: Validation of the Semiautomated Extraction Procedure

The semiautomated braided river pattern extraction methodology, developed in section 2, was tested and validated by comparing extracted river patterns to some form of ground truth. Typically, tracings of aerial photographs are accepted as valid ground truth. However, obtaining aerial photographs or ground-based observations of the same reaches of the Tanana River and at the same instants of time as on the ERS-1 SAR images was not feasible. Therefore the ground truth was taken as a tracing of a hardcopy of a full-resolution SAR image that was then digitized to produce an image consisting of black and white pixels, indicating the presence or absence of active channels. The question to be answered was could the semiautomated extraction method produce a braided river pattern comparable to a manual tracing in terms of visual appearance and spatial scaling analysis?

The scene used for verification was an ERS-1 SAR image taken on May 31, 1993, over the Tanana River, Alaska, just upstream of Fairbanks (reach A). The stages of image processing and image enhancement were automatically applied to that scene. Then, the manual stage of image classification was applied at three different levels. Level 1 involved ~30 min of manual image interpretation, while levels 2 and 3 involved an additional 15 min each. The incremental time between levels was used to consider more carefully tonal variation and to make the image more visually appealing (i.e., smoothing of channel edges and insuring complete channel connectivity). Obviously, the three levels correspond to different amounts of subjectivity and provide a means of testing the sensitivity of the spatial scaling results to subjective decisions in the extraction methodology. All images were subjected to the postimage processing stage applying the filtering discussed in section 2.

The extracted braided river patterns from semiautomated levels 1, 2, and 3, along with the pattern obtained by tracing, are shown in Figure 7. Visually, the level 3 pattern is most comparable to the digitized tracing, but visual comparison alone is not enough to validate the extraction methodology. Further validation involved comparing the spatial scaling results for the patterns obtained using the three levels of semiautomation to that of the traced pattern (which was considered the ground truth). For that purpose the logarithmic correlation method (LCI) of *Sapozhnikov and Foufoula-Georgiou* [1995] was applied to each of the patterns to test the presence of spatial scaling. The X axis was oriented in the streamwise direction and aligned to connect the upstream and downstream ends of the river reach. The Y axis was perpendicular to the X axis. From the correlation integral surface $z(x, y)$ the derivatives $\partial z(x, y)/\partial x$ and $\partial z(x, y)/\partial y$ were numerically computed from the part of the $z(x, y)$ surface corresponding to scales (Y) ranging between the smallest individual channel to the average width of the braidplain. The dependence of $\partial z(x, y)/\partial y$ versus $\partial z(x, y)/\partial x$ for each of the patterns is shown in Figure 8. The linear dependence (presence of scaling) is measured quantitatively by the correlation coefficient between $\partial z(x, y)/\partial y$ and $\partial z(x, y)/\partial x$ and the absolute error between the actual data points and the best fit line (or the spread of the cloud of points) (see Table 4). As can be seen from Figure 8a, which represents the ground truth, the cloud of points is well fitted by a straight line which confirms the presence of spatial scaling in this river pattern. Figures 8b, 8c, and 8d (see also Table 4) confirm also the presence of scaling for levels 1, 2, and 3 of the extraction methodology. The differences in the shape of the clouds reflect the subjectivities in the extraction methodology. Notice that in all cases the clouds of points are evenly distributed around the best fit lines and do not show the tendency of concavity as was the case in Figures 3b and 3c. The fact that scaling basically holds for all three of the extracted patterns is encouraging and verifies that the extraction methodology itself does not induce an artifical scaling break.

Despite the presence of scaling in all of the extracted patterns, there are some substantial qualitative differences be-

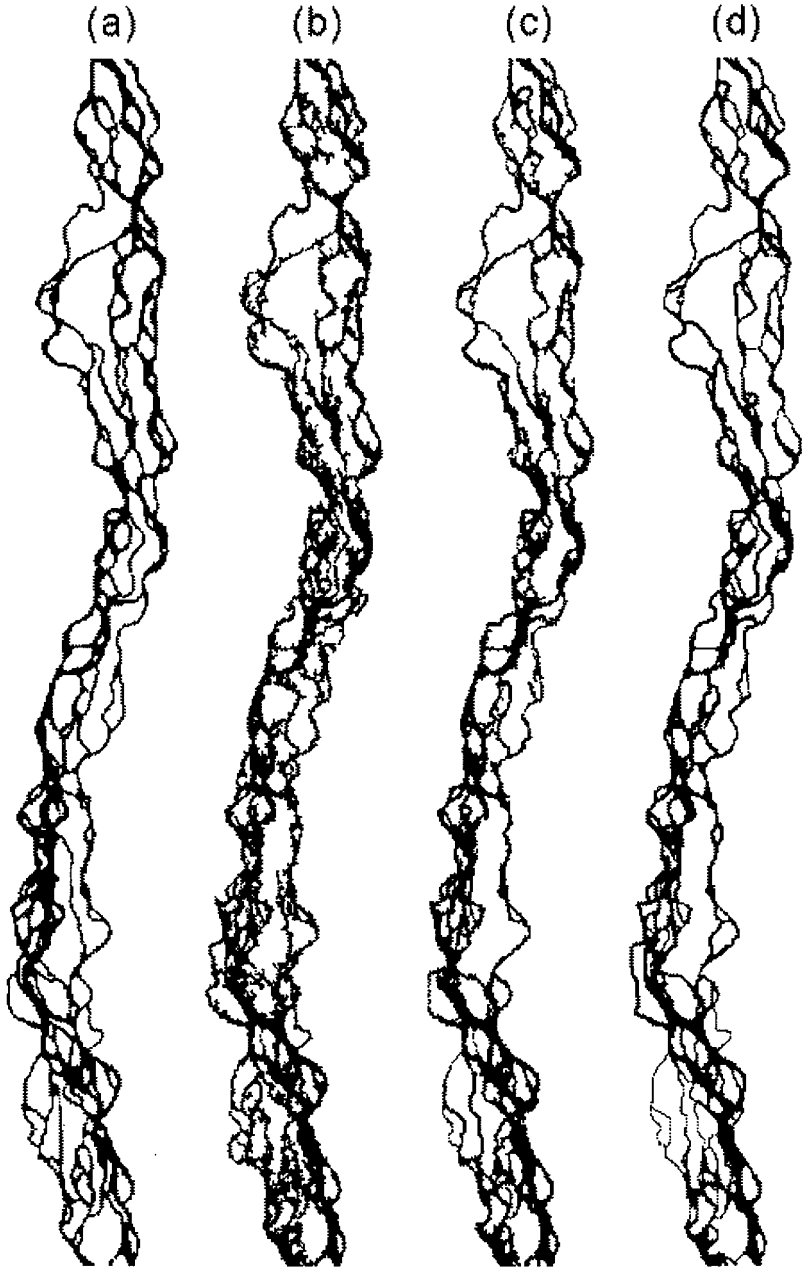

Figure 7. Braided river patterns of the Tanana River, reach A, image ID 152993100, for various extraction methodologies: (a) digitized tracing, (b) semiautomated level 1, (c) semiautomated level 2, and (d) semiautomated level 3.

tween the plots that correspond to the different extraction methodologies as compared to that of the ground truth. For example, the level 1 pattern (Figure 8b) does not include features which give $\partial z(x, y)/\partial y$, $\partial z(x, y)/\partial x$ values in the upper left region (boxed area) of the plot as do levels 2 and 3 and the traced patterns (see Figures 8a, 8c, and 8d). This region represents features which were most likely lost because of overfill into inactive channels, which caused jagged edges and discontinuity in the level 1 extracted pattern. This sensitivity in the level 1 pattern versus the level 2 and 3 patterns should be recognized and care should be taken in making the braided river patterns look somewhat natural. The similarity in the plots of the dependence of $\partial z(x, y)/\partial y$ versus $\partial z(x, y)/\partial x$ for semiautomated levels 2 and 3 to each other and to that of the traced pattern shows that once a reasonable pattern is obtained, further image cleanup, although producing a more visually appealing result, is insignificant for spatial scaling analysis and inferences. This signifies a robustness in the manual part of the semiautomated extraction procedure in that a few superfluous features (e.g., mild roughness and small gaps in connectivity) do not adversely affect the scaling analysis results.

To estimate the scaling exponents ν_x and ν_y, the best fit lines in the plots $\partial z(x, y)/\partial y$ versus $\partial z(x, y)/\partial x$ are needed. This was done using the algorithm of *Alciatore and Miranda* [1995] mentioned in section 3. The estimated scaling exponents are reported in Table 4 along with the measures of linear dependence. The ν_x and ν_y values were 0.72–0.75 and 0.44–0.48,

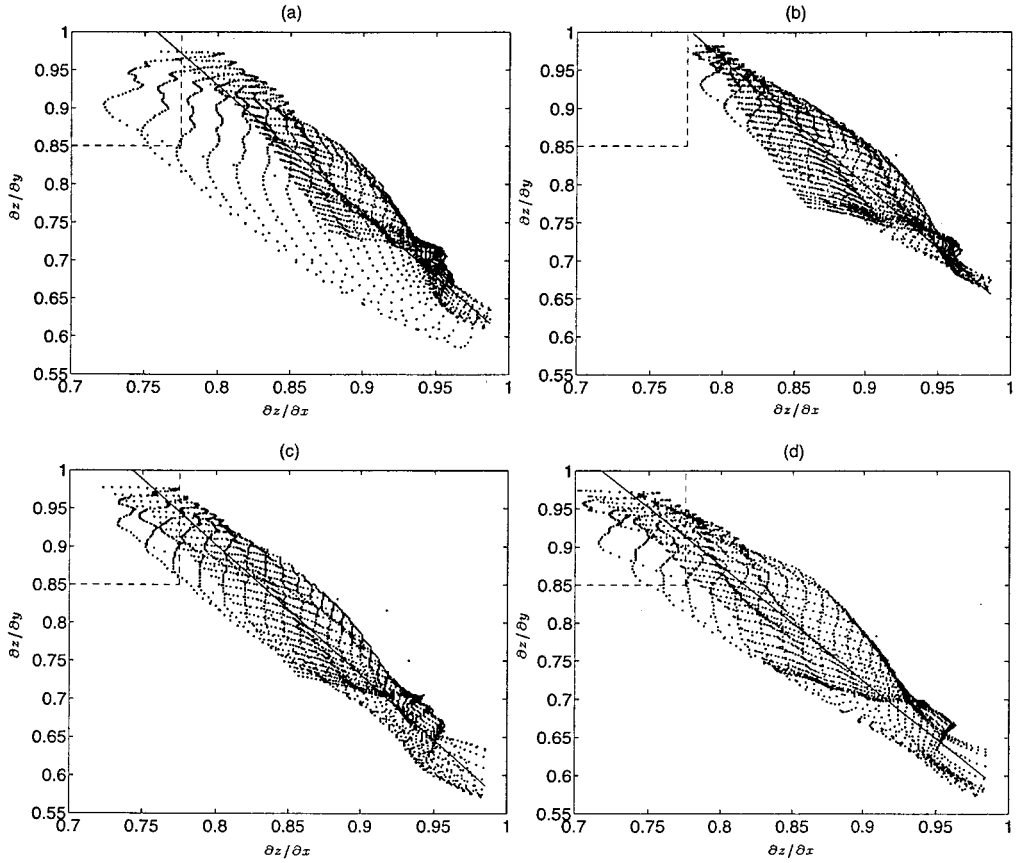

Figure 8. Dependence of $\partial z(x, y)/\partial y$ versus $\partial z(x, y)/\partial x$ for (a) digitized tracing, (b) semiautomated level 1, (c) semiautomated level 2, and (d) semiautomated level 3 of the Tanana River, reach A, image ID 152993100. Fractal exponents ν_x and ν_y are estimated from the best fit line and are shown in Table 4.

respectively. The closeness in spatial scaling exponents along with the visual similarity of the patterns validates the semiautomated braided river extraction methodology developed for use with full-resolution SAR images. The semiautomated procedure used for this study was constrained to greater than or equal to manual interpretation level 2.

Appendix B: Relationship of Discharge and Effective Width

Recently, *Smith et al*. [1995, 1996] derived for braided rivers an empirical relationship between discharge Q and "effective width" W_e, where W_e is defined as the total area covered by water in a control section divided by the length of that section. The relationship followed a typical power law form where W_e equalled a coefficient times the discharge raised to a power. The coefficient and discharge exponent were found to vary from river to river. These power functions were determined based on satellite-derived rating curves. *Smith et al*. [1996] derived such an empirical relationship for the Tanana River as

$$W_e = 50.45Q^{0.38} \tag{7}$$

where W_e is in meters and Q is in cubic meters per second.

The flow rates listed in Table 1 correspond to gaged measurements taken from the Tanana River at Fairbanks, Alaska. One of the four reaches analyzed in this study is located just upstream of Fairbanks. A test was performed to compare the W_e computed from the braided river patterns extracted using the semiautomated scheme to W_e computed using the known discharge and the relationship developed by *Smith et al*. [1996].

For example, the effective width calculated for the May 31, 1993, extracted braided river pattern from SAR was 608 m.

Table 4. Spatial Scaling for Various Extraction Methodologies

Scheme	ν_x	ν_y	Correlation Coefficient	Average |error|	Standard Deviation |error|
Traced	0.74	0.44	−0.895	0.0166	0.0152
SemiAutomated					
Level 1	0.72	0.44	−0.934	0.0125	0.0099
Level 2	0.75	0.44	−0.947	0.0144	0.0094
Level 3	0.72	0.48	−0.933	0.0179	0.0113

Using the derived $W_e - Q$ relationship and the known discharge of 35,300 cfs (1000 cubic meters per second), a W_e of 696 m was obtained. The difference between these two is ~90 m in terms of effective width. This is an acceptable range of error considering the resolution and geolocation accuracy of SAR and the fact that the $W_e - Q$ relationships are empirically derived. This difference in W_e corresponds to a difference in estimated discharge of 300 $m^3 s^{-1}$. The error in the relationship derived by *Smith et al*. [1996] for the Tanana River was stated to range from tens to hundreds of cubic meters per second. This is further evidence that the empirical relationship derived for the Tanana River holds within the specified range and with relative robustness to the braided river pattern used to compute W_e since the pattern used by Smith et al. and the pattern used here were derived in somewhat different ways [see *Smith et al*. 1995, 1996].

The measured flow rate of the October 18, 1993, scene is unknown. On the basis of the agreement between the W_e of the semiautomated extracted patterns with the relationships developed by *Smith et al*. [1996] the discharge for this scene can be estimated using the computed effective width. The discharge estimated using (7) was 220 $m^3 s^{-1}$ (or 7800 $ft^3 s^{-1}$).

Acknowledgments. This research was supported by NSF grant EAR-9628393 and NASA grant NAG5-6191. ERS-1 data were acquired by the European Space Agency and provided by NASA through the Alaska SAR Facility. We thank the Minnesota Supercomputer Institute for providing computer facilities for our research. We also thank J. Bell, of the University of Minnesota, who allowed our use of computing facilities for image processing and L. Smith of the Department of Geography, UCLA, for helpful discussions and insights regarding SAR applications.

References

Alciatore, D., and R. Miranda, The best least-squares line fit, in *Graphics Gems V*, edited by A. W. Paeth, pp. 91–97, Academic, San Diego, Calif., 1995.

Ashmore, P., and G. Parker, Confluence scour in coarse braided streams, *Water Resour. Res*., *19*, 392–402, 1983.

Ashmore, P. E., R. I. Ferguson, K. L. Prestegaard, P. J. Ashworth, and C. Paola, Secondary flow in anabranch confluences of a braided, gravel-bed stream, *Earth Surf. Processes Landforms*, *17*, 299–311, 1992.

Beauvais, A. A., and D. R. Montgomery, Influence of valley type on the scaling properties of river planforms, *Water Resour. Res*., *32*, 1441–1448, 1996.

Best, J. L., The morphology of river channel confluences, *Prog. Phys. Geogr*., *10*, 157–174, 1986.

Best, J. L., Sediment transport and bed morphology at river channel confluences, *Sedimentology*, *35*, 481–498, 1988.

Bristow, C. S., J. L. Best, and A. G. Roy, Morphology and facies models of channel confluences, in *Alluvial Sedimentation*, edited by M. Marzo and C. Puigdefabregas, pp. 91–100, Blackwell Sci., Cambridge, Mass., 1993.

Frost, V. S., J. A. Stiles, K. S. Shanmugan, and J. C. Holtzman, A model for radar images and its application to adaptive digital filtering of multiplicative noise, *IEEE Trans. Pattern Anal. Mach. Intel*., *4*, 157–166, 1982.

Hagg, W., and M. Sties, Efficient speckle filtering of SAR images, in *International Geoscience and Remote Sensing Symposium*, vol. 4, pp. 2140–2142, Calif. Inst. of Technol., Pasadena, 1994.

Jensen, J. R., *Introductory Digital Image Processing: A Remote Sensing Perspective*, Prentice Hall, Englewood Cliffs, N. J., 1996.

La Barbera, P., and R. Rosso, On the fractal dimension of stream networks, *Water Resour. Res*., *25*, 735–741, 1989.

Lopes, A., R. Touzi, and E. Nezry, Adaptive speckle filters and scene heterogeneity, *IEEE Trans. Geosci. Remote Sens*., *28*, 992–1000, 1990.

Mosley, M. P., An experimental study of channel confluences, *J. Geol*., *84*, 535–562, 1976.

Mosley, M. P., Stream junctions: A probable location for bedrock placers, *Econ. Geol*., *72*, 691–697, 1977.

Murray, A. B., and C. Paola, A cellular model of braided rivers, *Nature*, *371*, 54–57, 1994.

Nikora, V. I., Fractal structures of river plan forms, *Water Resour. Res*., *27*, 1327–1333, 1991.

Nikora, V. I., D. M. Hicks, G. M. Smart, and D. A. Noever, Some fractal properties of braided rivers, paper presented at Second International Symposium on Fractals and Dynamic Systems in Geoscience, Johann Wolfgang Goethe-Univ., Frankfurt am Main, Germany, 1995.

Nykanen, D. K., Study of the morphology and spatial scaling of braided rivers using synthetic aperture radar imagery, M. S. thesis, Univ. of Minnesota, Minneapolis St. Paul, 1997.

Oliver, C. J., Information from SAR images, *J. Phys. D Appl. Phys*., *24*, 1493–1514, 1991.

Olmsted, C., Alaska SAR facility scientific user's guide, *Rep. ASF-SD-003*, Alaska SAR Facility, Fairbanks, July 1993.

Peckham, S. D., New results for self-similar trees with application to river networks, *Water Resour. Res*., *31*, 1023–1029, 1995.

Robert, A., Bed configuration and microscale processes in alluvial channels, *Prog. Phys. Geogr*., *17*, 123–136, 1993.

Sapozhnikov, V. B., and E. Foufoula-Georgiou, Study of self-similar and self-affine objects using logarithmic correlation integral, *J. Phys. A Math. Gen*., *28*, 559–571, 1995.

Sapozhnikov, V. B., and E. Foufoula-Georgiou, Self-affinity in braided rivers, *Water Resour. Res*., *32*, 1429–1439, 1996.

Sapozhnikov, V. B., and E. Foufoula-Georgiou, Experimental evidence of dynamic scaling and indications of self-organized criticality in braided rivers, *Water Resour. Res*., *33*, 1983–1991, 1997.

Sapozhnikov, V. B., and V. I. Nikora, Simple computer model of a fractal river network with fractal individual watercourse, *J. Phys. A Math. Gen*., *26*, L623–L627, 1993.

Shi, Z., and K. B. Fung, A comparison of digital speckle filters, in *Proceedings of the International Geoscience and Remote Sensing Symposium*, vol. 4, pp. 2129–2133, Calif. Inst. of Technol., Pasadena, 1994.

Smith, L. C., B. L. Isacks, R. R. Forster, A. L. Bloom, and I. Presuss, Estimation of discharge from braided glacial rivers using ERS 1 synthetic aperture radar: First results, *Water Resour. Res*., *31*, 1325–1329, 1995.

Smith, L. C., B. L. Isacks, A. L. Bloom, and A. B. Murray, Estimation of discharge from three braided rivers using synthetic aperture radar satellite imagery: Potential applications to ungaged basins, *Water Resour. Res*., *32*, 2031–2034, 1996.

Tarboton, D. G., R. L. Bras, and I. Rodriguez-Iturbe, The fractal nature of river networks, *Water Resour. Res*., *24*, 1317–1322, 1988.

E. Foufoula-Georgiou, D. K. Nykanen, and V. B. Sapozhnikov, St. Anthony Falls Laboratory, Mississippi River at Third Avenue SE, University of Minnesota, Minneapolis, MN 55414-2196. (e-mail: efi@mykonos.safhl.umn.edu; deborah@mykonos.safhl.umn.edu; sapoz001@maroon.tc.umn.edu)

(Received August 1, 1997; revised March 13, 1998; accepted March 17, 1998.)